Zhiyi Cao
Department of Aerospace Engineering and Engineering Mechanics,
Research Center for the Mechanics of Solids, Structures and Materials,
The University of Texas at Austin,
Austin, TX 78712

Li Tao
Department of Electrical and Computer Engineering,
The University of Texas at Austin,
Austin, TX 78712

Deji Akinwande
Department of Electrical and Computer Engineering,
The University of Texas at Austin,
Austin, TX 78712

Rui Huang
Department of Aerospace Engineering and Engineering Mechanics,
Research Center for the Mechanics of Solids, Structures and Materials,
The University of Texas at Austin,
Austin, TX 78712

Kenneth M. Liechti[1]
Department of Aerospace Engineering and Engineering Mechanics,
Research Center for the Mechanics of Solids, Structures and Materials,
The University of Texas at Austin,
Austin, TX 78712

Mixed-Mode Interactions Between Graphene and Substrates by Blister Tests

Many of the attractive properties of graphene will only be realized when it can be mass produced. One bottleneck is the efficient transfer of graphene between various substrates in nanomanufacturing processes such as roll-to-roll and transfer printing. In such processes, it is important to understand how the ratio of shear-to-tension at the interface between graphene and substrates affects the adhesion energy. With this in mind, this paper examines the mixed-mode adhesive interactions between chemical vapor deposition (CVD) grown graphene that had been transferred to copper or silicon substrates. The approach that was taken was to use blister tests with a range of graphene backing layer materials and thicknesses in order to provide a wide range of the shear-to-tension ratio or fracture mode-mix at the interface. Raman spectroscopy was used to ensure that graphene had indeed been delaminated from each substrate. Measurements of pressure, top surface deflection, and blister diameter were coupled with fracture mechanics analyses to obtain the delamination resistance curves and steady state adhesion energy of each interface. The results showed that the adhesive interactions between graphene and both substrates (Cu and Si) had a strong dependence on the fracture mode-mix. In the absence of plasticity effects, the most likely explanation of this effect is asperity locking from the inherent surface roughness of the substrates. [DOI: 10.1115/1.4030591]

1 Introduction

Graphene has been found to have extraordinary optoelectronic and mechanical properties that have attracted much attention in a wide range of potential applications. Typically, large-area CVD grown graphene will need to be removed from its seed substrate and transferred to target substrates of interest; both the removal and transfer steps require a fundamental understanding of the adhesive behavior between graphene and the substrates. The adhesion energy of graphene on various substrates has been measured by several research groups. By intercalating nanoparticles between graphene and silicon, Zong et al. [1] reported the adhesion energy to be 0.151 J/m^2. Koeing et al. [2] measured the adhesion of micromechanically exfoliated graphene on SiO_2, obtaining 0.45 J/m^2 for monolayer graphene and 0.31 J/m^2 for two to five layered graphene. Under nominally similar conditions, Boddeti et al. [3] found the adhesion energy for the graphene/silicon interface to be 0.250 J/m^2, which suggests some variability in these measurements. Cao et al. [4] measured the adhesion energy of CVD grown graphene transferred to copper substrates using a large scale blister test, obtaining a steady state adhesion energy of 0.341 J/m^2. Na et al. [5] used wedge tests and infrared interferometry method to measure the strength, range, and adhesion energy of interactions between transferred graphene on silicon and found it to be 0.357 J/m^2. The adhesion energy between graphene and its seed copper is higher [6,7]. The range of adhesion energies for graphene that has been transferred to silicon and copper might be due to contamination, surface roughness, or liquid trapped between the graphene and the substrate, as several authors have suggested [2,5,8,9]. However, one more reason for these variations is the potential dependence of the adhesion energy on the ratio of shear-to-tensile stresses at the interface, also known as the fracture mode-mix, which was not considered in any of the previous experiments and can vary from one test configuration to another.

Interfacial fracture mechanics focuses on crack growth between two materials. This form of crack growth is common in many engineering applications, such as adhesive joints, fiber-reinforced composites, and thin film coatings [10–12]. As summarized in the review of interfacial fracture mechanics [13], the mismatch of the material properties and the fact that the crack is constrained to grow along the interface dictates that the interfacial fracture energy in general depends on both tensile and shear stresses. In classical fracture mechanics parlance, interfacial fracture is governed by a combination of local mode I (tension) and modes II and III (forward and out-of-plane shear) effects. Dundurs' pioneering work established two parameters that capture the elastic mismatch of a bimaterial pair [14]. The complex singularity near crack tips resulting from small strain, linearly elastic stress analyses predicts wildly oscillating stresses and interpenetration of crack faces, phenomena which are not encountered in the fracture of homogeneous materials. Nonetheless, Rice [15] was able to put these phenomena in perspective and develop a working description of the stresses and displacements near interfacial crack tips. Suo and Hutchinson [16] derived a series of formulas for the energy release rate and stress intensity factors for mixed-mode interfacial cracks. In general, the interfacial fracture toughness depends on the mode-mix, where the fracture mode-mix is defined by a phase angle depending on the ratio between the shear and tensile stress intensity factors with a particular length scale for the

[1]Corresponding author.

Contributed by the Applied Mechanics Division of ASME for publication in the JOURNAL OF APPLIED MECHANICS. Manuscript received April 1, 2015; final manuscript received May 7, 2015; published online June 9, 2015. Editor: Yonggang Huang.

 Copyright © 2015 by ASME

Downloaded From: http://appliedmechanics.asmedigitalcollection.asme.org/ on 06/12/2015 Terms of Use: http://asme.org/terms

interfacial crack. Often, the interfacial toughness rises as the contribution from mode II increases. Wang and Suo [17] conducted fracture tests on metal/epoxy systems and obtained higher toughness values at larger phase angles. Chai and Liechti [18] measured the toughness of a glass/epoxy interface over a wide range of mode-mix. A strong toughening effect was observed with increasing shear components (positive and negative). Several potential contributions to the toughening effect have been discussed. Evans and Hutchinson [19] proposed an analytical model based on asperity locking along the fracture interfaces. Swadener and Liechti [20] carried out an analysis on the crack of glass/epoxy interface and concluded that plastic dissipation accounted for the toughening. Additional mechanisms such as viscoelasticity can be seen in Ref. [21]. In many of the experiments, devices that could apply biaxial loading conditions were used to control loading paths with various tension and shear combinations. In this study, a simple blister test was used. Different mode-mixes were achieved by varying the stiffness of the blister layer. This has been alluded to by Jensen and Thouless [22,23] who considered pressurized blisters and showed that a range of negative mode-mixes could be obtained. Here, it is found that positive mode-mixes can be obtained by using laminated blister films with a very compliant layer at the substrate/blister interface, thereby greatly extending the range of mode-mix available to the blister test.

In this paper, we present a series of blister tests for photoresist/polydimethylsiloxane (PDMS) and photoresist/PDMS/graphene laminated films placed on copper and silicon substrates. Full field interferometry measurements were carried out to measure the blister profiles. Numerical simulations were carried out to establish how the mode-mix might be controlled by changing the thicknesses of the photoresist and PDMS layers. Delamination resistance curves were obtained for different interfaces, and the adhesion energies of graphene/copper and graphene/silicon interfaces were determined as a function of mode-mix. Raman spectroscopy was used to identify the delaminated interface and determine the quality of graphene following delamination.

2 Experimental

A schematic of the blister test is shown in Fig. 1. The film is pressurized with deionized water through a hole in the substrate using a syringe pump operating in volume control. The deflection of the free surface of the film is measured with an interference objective at the same time as the pressure is measured by a pressure transducer. The details of the apparatus, image, and data processing can be found in our previous paper [4]. The main modification for the present work was the use of a PDMS layer in the film, which required some changes in the experiment and analysis.

2.1 Sample Preparation. In the previous study [4], photoresist was used as a backing layer for graphene. However, it was determined that the photoresist had a peak in its Raman spectrum that was very close to the G peak for graphene, thereby obscuring the assessment of the quality of the graphene. For this study, PDMS (Sklgard 184, silicone) was coated on graphene directly, because it does not generate as much background noise as photoresist does in Raman spectra [4]. However, photoresist (MicroChem Corporation, Westborough, MA, SU-8 2035) was still needed here, because the blister deflection would otherwise be out of the measurement range of the interferometer. A second set of specimens consisting of the same PDMS and photoresist but without graphene was tested as a control.

The graphene that was used in this study was produced by CVD [24]. Then it was transferred [25] to copper films, roughly 100 nm thick, which had been deposited on a silicon wafer using a Denton thermal evaporation system. The operating pressure was approximately 10^{-6} Torr, and the deposition rate was 1 Å/s.

PDMS consists of a base and a cross-linker which were mixed in a 10:1 weight ratio to achieve a fully cross-linked elastomer. The mixture was stirred for 5 min and then put in a vacuum desiccator to degas for 20 min. The PDMS was then spun on top of the graphene at 3000 rpm for 35 s. The sample was then cured at 75 °C for 2 hrs. The nominal thickness of the PDMS ranged from 10 to 50 μm. For each specimen, the thickness was measured using a profilometer (Dektak6M) with a vertical range and resolution of 260 μm and 10 nm, respectively. The photoresist was then spun on top of the PDMS for 35 s at 3700 rpm to a nominal thickness of 40 μm. In some cases, a thinner (Su-8 2000) was added to the photoresist as a solvent to produce layers of 10–20 μm by varying the solvent concentration. After curing, a razor blade was used to cut 1×1-cm grids on the laminated graphene/PDMS/photoresist film. The assembly was then submerged in an ammonium persulfate solution (1.0 wt. %). The etchant flowed into the trenches to etch away the copper film underneath the graphene. This process took 3–4 hrs. Subsequently, all the small squares of the laminated films were rinsed in deionized water. In this way, optically flat graphene/PDMS/photoresist films were obtained and each square was used to produce a circular blister. The same process was used to produce PDMS/photoresist films without graphene.

The next step was to transfer the square film over a hole in a substrate to produce a suspended film. Copper and silicon substrates were used here. The copper substrate was made of 101 oxygen-free, high-conductivity copper (Trident, Inc., Richardson, TX). The hole in the copper substrate was mechanically drilled with a diameter of 544 μm. The surface of the substrate was then polished by a range of sandpapers, and 3, 1, and 0.05 μm diamond compound pastes, until it was mirrorlike. Deionized water and acetone were applied to clean the surface after polishing. The substrate was then scanned by atomic force microscopy. The root-mean-squared (RMS) roughness was about 5 nm over a $10 \times 10\,\mu$m area at approximately 0.15 mm from the edge of the hole. The Si (111) substrate had a hole whose diameter was 832 μm, which was produced by laser-drilling (Potomac Photonics, Inc., Baltimore, MD). The silicon surface in the vicinity of the hole was not damaged by the drilling process. It was cleaned by deionized water and acetone before the laminated films were transferred onto it. Its RMS roughness was less than 0.4 nm.

After the transfer, the specimen was baked at 75 °C for 15 min with pressure being applied to the film via a small weight (approximately 100 g). The temperature was chosen to be the same as the curing temperature for PDMS so that the flow of PDMS could improve the contact between the film and the substrate. The weight helped improve the contact between the film and the substrates.

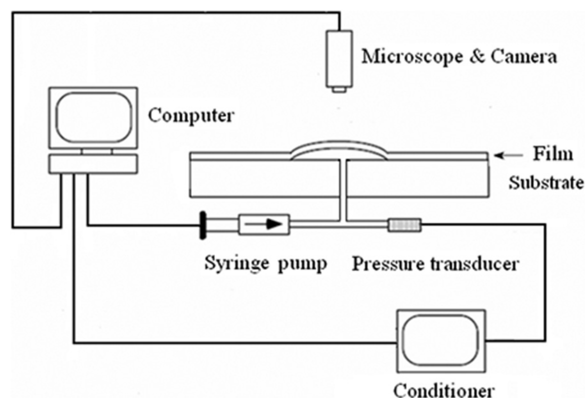

Fig. 1 Schematic of the blister test apparatus

2.2 Blister Deflection. After attaching the specimen to the pressure manifold with a rubber O-ring seal, the assembly was placed under the microscope (Fig. 1). The distance between the interference objective and the specimen was carefully adjusted so

Downloaded From: http://appliedmechanics.asmedigitalcollection.asme.org/ on 06/12/2015 Terms of Use: http://asme.org/terms

that fringe patterns were visible. At this time, the tilt of the reference mirror in the interference objective was also adjusted to establish proper alignment. Deionized water was then injected at a rate of 5 ml/hr in order to pressurize the blister. At zero pressure, the suspended film was slack and drooped slightly below the substrate surface. The possible reasons were discussed in Ref. [4]. In subsequent analyses of the blister profiles, deflections were measured with respect to this initial state.

An example interferogram of a graphene/PDMS/photoresist blister on copper at 45.4 kPa pressure is shown in Fig. 2. The initial diameter of the blister was 544 μm. The crack had propagated slightly at this pressure, as indicated by the crack front location. The crack front is visible as a thin black line in the interferogram. Each fringe represents a height contour of the outer surface of the blister. The height interval between two successive dark fringes was 275 nm (half wavelength of green light). Due to the large compliance of PDMS, the deflection of the upper surface of the blister extended far beyond the crack front. As the pressure increased, more and more circular fringes were generated. Delamination between the film and the substrate initiated at a critical pressure and remained stable until a second critical pressure was reached, at which point the delamination became unstable and the film was blown off. Before the blowoff, the delamination propagated rapidly for approximately 2 s. Stopping water injection did not arrest the unstable propagation. During the whole process, distinguishable fringes were apparent all over the blister, thereby enabling whole field measurement of the blister profiles. The film thickness was optimized to ensure that the full range of deflections could be measured within the range of the pressure transducer. Raman spectroscopy was used to determine the delamination path and quality of the graphene once the graphene/PDMS/photoresist film had completely delaminated.

3 Analysis

In previous analyses of blister specimens [4,26], the diameter-to-thickness ratio allowed the use of linear and nonlinear plate theories. However, in the specimens that were used in the present study, the diameter was smaller and the layer thickness was larger, which precluded the use of plate theories. Accordingly, finite element analysis was employed for the fracture analysis of the specimens using the commercial package ABAQUS®. All material components were taken to be linearly elastic and isotropic (Table 1). Energy release rates and stress intensity factors were determined by postprocessing routines in ABAQUS.

The finite element model (Fig. 3) was axisymmetric with $h_{\rm PR}$ and $h_{\rm PDMS}$ denoting the thickness of photoresist and PDMS, respectively. The radius of the hole in the substrate was a_0 and Δa was the increment in the blister radius due to delamination. The

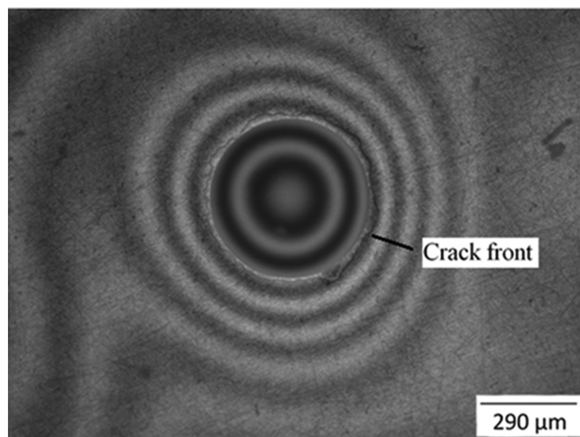

Fig. 2 An interferogram of a graphene/PDMS/photoresist blister on copper at 45.4 kPa

Table 1 Mechanical properties used in the finite element analysis

Material	Young's modulus E	Poisson's ratio ν
Copper	117 GPa	0.36
Silicon	160 GPa	0.22
PDMS	0.8 MPa	0.5
Photoresist	3.4 GPa	0.35

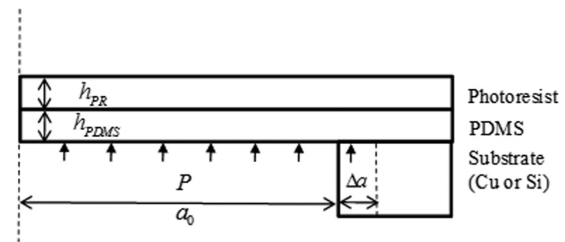

Fig. 3 The geometry and boundary conditions that were used in the finite element model

outer radius of the substrate was 1000 μm, much greater than the largest blister radius considered. The substrate was either copper or silicon, and its thickness was 80 μm. Graphene was not included in the model, because it was extremely thin compared to the other layers. Except for the delaminated portion, perfect bonding was imposed at the photoresist/PDMS and PDMS/substrate interfaces, making this a linearly elastic fracture mechanics model, where any process or sliding zones are assumed to be small. Uniform pressure was applied to the blister and between the crack faces. A series of models with different blister radii $(a = a_0 + \Delta a)$ were assembled to calculate the energy release rate and mode-mix. Quadrilateral elements (CAX8R) with reduced integration were used throughout the body except in the vicinity of the crack tip, where a set of quarter point singular elements were used to capture the stress singularity. Based on the observation that deflection of the outer surface of the blister extended well beyond the crack front, nonlinear geometrical analysis was incorporated in the simulations in order to account for potentially large deformations of the compliant PDMS. The J-integral, interfacial stress intensity factors, and fracture mode-mix were obtained using the interactive integral approach [27]. A suitable level of mesh refinement was established by convergence of the J-integral values, and it was determined that large deformations in the PDMS increased the J-integral values by 0.8%.

For reference, a brief summary of interfacial fracture mechanics concepts [13] is presented here. If E_i, μ_i, ν_i are the tensile and shear moduli and Poisson's ratios of the two materials $(i = 1, 2)$ across the interface, the Dundurs' elastic mismatch parameters are

$$\alpha = \frac{\overline{E}_1 - \overline{E}_2}{\overline{E}_1 + \overline{E}_2} \quad \text{and} \quad \beta = \frac{1}{2}\frac{\mu_1(1-2\nu_2) - \mu_2(1-2\nu_1)}{\mu_1(1-\nu_2) + \mu_2(1-\nu_1)} \tag{1}$$

where $\overline{E}_i = E_i/\left(1-\nu_i^2\right)$ in plain strain (also axisymmetric) and $\overline{E}_i = E_i$ in plane stress. The parameter α approaches 1 when the upper material $(i = 1)$ is extremely stiff compared to the lower one $(i = 2)$, and approaches -1 when the upper material is extremely compliant. Both α and β are 0 when there is no elastic mismatch. For blisters with PDMS, α and β were close to -1 and 0, respectively, because $\nu_{\rm PDMS} \approx 0.5$ and $E_{\rm PDMS} \ll E_s$.

The complex stress intensity factor for an interfacial crack is

$$K = K_1 + iK_2 \tag{2}$$

where the real and imaginary parts are K_1 and K_2. The normal and shear stresses directly ahead of the crack tip can be written in complex form as

Downloaded From: http://appliedmechanics.asmedigitalcollection.asme.org/ on 06/12/2015 Terms of Use: http://asme.org/terms

$$\sigma_{22} + i\sigma_{12} = (K_1 + iK_2)(2\pi r)^{-0.5} r^{i\varepsilon} \quad (3)$$

where $\varepsilon = [1/(2\pi)]\{\ln[(1-\beta)/(1+\beta)]\}$ is the bimaterial constant and r is the distance from the crack front. The phase angle of mode-mix is defined as

$$\psi = \tan^{-1}\left[\frac{\mathrm{Im}(Kl^{i\varepsilon})}{\mathrm{Re}(Kl^{i\varepsilon})}\right] \quad (4)$$

where l is an arbitrary length scale which was taken to be h_{PR} for specimens without PDMS. Since β was close to 0 in the blisters with PDMS, the bimaterial constant ε is approximately zero, making the choice of length scale inconsequential.

The J-integral or energy release rate is related to the stress intensity factors through

$$G = \frac{1}{2}(1-\beta^2)\left(\frac{1}{\overline{E}_{\mathrm{PDMS}}} + \frac{1}{\overline{E}_s}\right)(K_1^2 + K_2^2) \quad (5)$$

Values obtained from Eq. (5) differed from those obtained by the J-integral calculation in ABAQUS by less than 1% in all simulations.

4 Results and Discussion

First, we determined the Young's moduli of PDMS and photoresist by comparing the measured blister profiles with solution from the finite element model. Once this was accomplished, the analysis was generalized in order to conduct a parametric study that would allow experimental data to be quickly analyzed using a set of dimensionless parameters. The effects of material properties and specimen geometry on the fracture mode-mix were investigated in order to extend the commonly accepted range of mode-mix [23] available to the blister test. The results were then applied to a number of experiments that were conducted to explore any variations in adhesion energy of graphene with mode-mix.

The sensitivity of the deflection of the outer surface of the blister to the Young's moduli of the PDMS and photoresist was exploited to determine E_{PDMS} and E_{PR}. As mentioned in Sec. 2, the surface deflection extended beyond the crack front (Fig. 2) because of the high compliance of the PDMS layer. This phenomenon was also observed in the finite element solutions. As shown in Fig. 4(*a*), while the inner surface of the blister was deflected up to the crack front ($r/a \leq 1$), the deflection of the outer surface remains appreciable in an annular region beyond the crack front ($1 \leq r/a \leq 1.6$). To compare with the measured deflection of the outer surface, we conducted a parametric study of the effect of the moduli of the PDMS and photoresist. Varying the modulus of the photoresist resulted in notable differences in the central deflection of the blister (Fig. 4(*a*)) but had little effect on the deflection beyond the crack front ($r/a > 1$). On the other hand, the effect of stiffness of PDMS was significant beyond the crack front (Fig. 4(*b*)), where both the deflection and the radius at which it became zero were reduced with higher values of E_{PDMS}. As a result, the modulus of the PDMS was determined first by matching the surface deflection beyond the crack front, after which the photoresist modulus was determined by matching the central deflection. Using this approach, the moduli of the photoresist and PDMS were found to be 3.4 GPa and 0.8 MPa, respectively, which are in good agreement with previously published values [28]. The Poisson's ratios were taken to be 0.5 for PDMS and 0.35 for the photoresist in all simulations.

The energy release rate for the interfacial crack of the blister can be written in dimensionless form as

$$G = f\left(\frac{a}{h_{\mathrm{PR}}}, \frac{h_{\mathrm{PDMS}}}{h_{\mathrm{PR}}}, \alpha, \beta, \frac{E_{\mathrm{PR}}}{E_S}\right)\frac{p^2 h_{\mathrm{PR}}}{E^*} \quad (6)$$

where $E^* = \left\{\left[(1-\nu_{\mathrm{PDMS}}^2)/(E_{\mathrm{PDMS}})\right] + \left[(1-\nu_s^2)/(E_s)\right]\right\}^{-1}$. The functional form of the normalized energy release rate $GE^*/p^2 h_{\mathrm{PR}}$ was determined by conducting a series of analyses for a range of crack lengths for Cu and Si substrates (Fig. 5). As a result of the normalization and the small difference in the substrate moduli, the energy release rates for both substrates could be represented by the same function for a given value of $h_{\mathrm{PDMS}}/h_{\mathrm{PR}}$. For example, a cubic polynomial in a/h_{PR}

$$\frac{GE^*}{p^2 h_{\mathrm{PR}}} = 0.036\left(\frac{a}{h_{\mathrm{PR}}}\right)^3 - 0.0695\left(\frac{a}{h_{\mathrm{PR}}}\right)^2 + 0.694\left(\frac{a}{h_{\mathrm{PR}}}\right) - 1.8078 \quad (7)$$

gave the best fit to the finite element results for $h_{\mathrm{PDMS}}/h_{\mathrm{PR}} = 2.38$. By substituting measured pressure levels and blister radii into Eq. (7), the energy release rate at any point of time in an experiment could be obtained. Similar polynomial fits

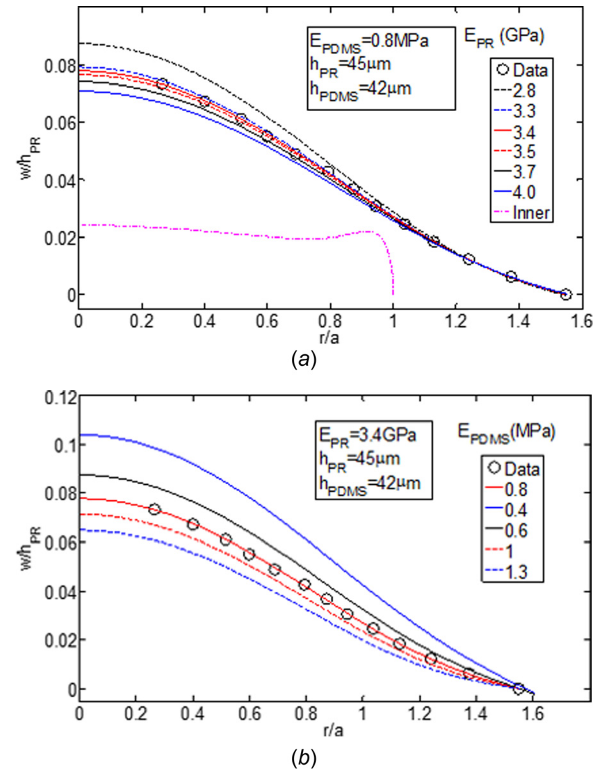

Fig. 4 Comparison of the surface deflection profiles between experiment and finite element simulations using different moduli for PDMS and photoresist. The pressure was 76.2 kPa and the crack length $a = 285\,\mu$m. (*a*) Varying E_{PR} when $E_{\mathrm{PDMS}} = 0.8$ MPa and (*b*) varying E_{PDMS} when $E_{\mathrm{PR}} = 3.4$ GPa.

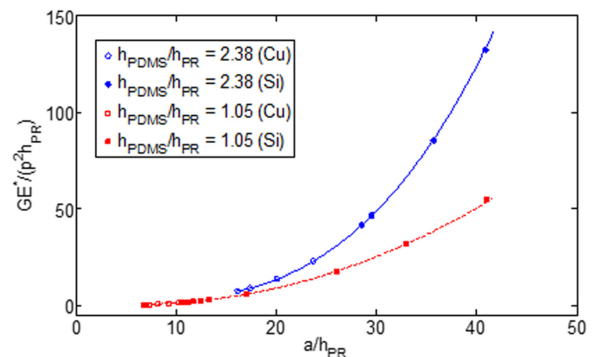

Fig. 5 Normalized energy release rate of an interfacial delamination as a function of the normalized crack length

Downloaded From: http://appliedmechanics.asmedigitalcollection.asme.org/ on 06/12/2015 Terms of Use: http://asme.org/terms

Table 2 **Coefficients for Eq. (7) as a function of PDMS/photoresist thickness**

h_{PDMS}/h_{PR}	C_1	C_2	C_3	C_4
0.425	0.0012	−0.0125	0.0525	5.9729
1.05	0.0003	0.0266	−0.2369	0.8142
2.38	0.0036	−0.0695	0.694	−1.8078
2.86	0.0105	−0.2424	2.1276	−3.5903

were obtained for other thickness ratios, and the corresponding coefficients are presented in Table 2.

The effects of geometry and material properties on the mode-mix are shown in Fig. 6. As defined in Eq. (4), the mode-mix phase angle is a dimensionless function characterizing the ratio between shear and tensile stresses ahead of the crack front. For the blister tests in the present study, dimensional considerations suggest that

$$\psi = \psi\left(\frac{a}{h_{PR}}, \frac{h_{PDMS}}{h_{PR}}, \alpha, \beta\right) \quad (8)$$

Figure 6(*a*) shows that the fracture mode-mix was independent of the crack length for the PDMS/graphene/copper and PDMS/graphene/silicon specimens considered in this study. Thus, in each blister test, the mode-mix did not vary during the delamination process, thereby allowing the adhesion energy for a given mode-mix to be obtained for each specimen. For blister tests with bare photoresist films, the Dundurs' parameters for the interface are different with a nonzero value of β. As a result, the mode-mix angle depends on the choice of a length scale following the definition given in Eq. (4), taking the form

$$\psi = \psi\left(\frac{a}{h_{PR}}, \frac{l}{h_{PR}}, \alpha, \beta\right) \quad (9)$$

By taking $l = h_{PR}$, the phase angle for the photoresist/Cu interface is only a function of a/h_{PR} (Fig. 6(*b*)). While this is a somewhat arbitrary choice of length scale, another length scale (say l_1) can easily be incorporated through the transformation $\psi_1 = \psi + \varepsilon \ln(l_1/l)$ [13]. In this case, the mode-mix does change during the delamination process. However, for each specimen, the amount of crack growth was relatively small so that the mode-mix was approximately constant. On the other hand, by changing the thickness h_{PR} of the photoresist, it is possible to achieve mode-mix values ranging from −20 deg to −60 deg.

It is interesting to note that the signs of the mode-mix were opposite for the blister tests using the PDMS/photoresist and bare photoresist films. As shown in Fig. 7, the shear stress distributions around the crack front differ dramatically for the cases with and without PDMS. In the latter case, the shear stress straight ahead of the crack is negative and thus the phase angle is negative, similar to previous studies of blister tests using relatively stiff films [23]. However, when a PDMS layer is inserted, the shear stress becomes positive so that the phase angle becomes positive. This is largely due to the compliance of PDMS. Consequently, the deformation near the crack front is much larger than with the bare photoresist, as can be seen from the crack opening in Fig. 7(*a*) as well as Fig. 4(*a*). The effect of PDMS compliance is further examined in Fig. 6(*c*), where the phase angle decreases with increasing PDMS modulus and becomes negative when $E_{PDMS} = 800$ MPa. Thus, by using a compliant layer with different elastic moduli, a wide range of mode-mix can be achieved in the blister test. Figure 6(*d*) shows the dependence of mode-mix on the thickness ratio h_{PDMS}/h_{PR} for the two cases with PDMS. Within the range of thickness accessible to spin-coating, the mode-mix was mainly

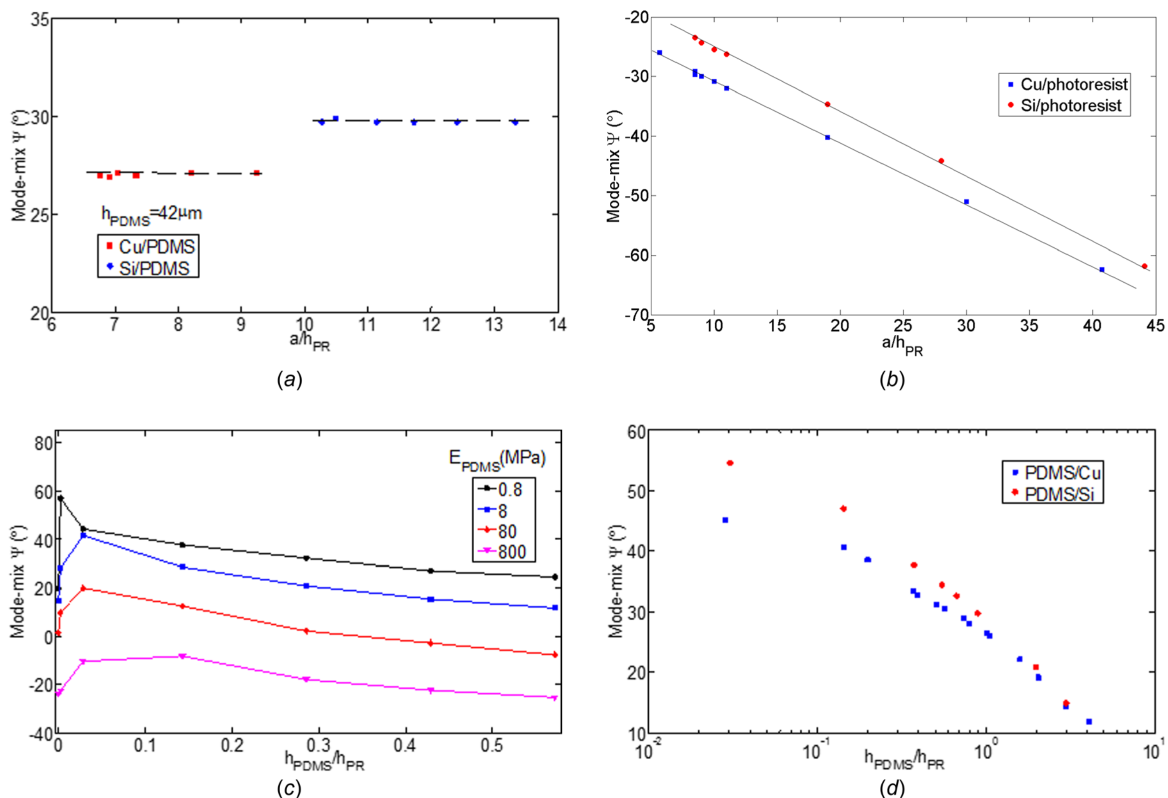

Fig. 6 (*a*) Fracture mode-mix versus normalized crack length for blister tests with PDMS; (*b*) the phase angle of mode-mix for blister tests with bare photoresist; (*c*) effect of Young's modulus of PDMS on mode-mix; and (*d*) dependence of the mode-mix on the layer thickness ratio for blister tests with PDMS

Downloaded From: http://appliedmechanics.asmedigitalcollection.asme.org/ on 06/12/2015 Terms of Use: http://asme.org/terms

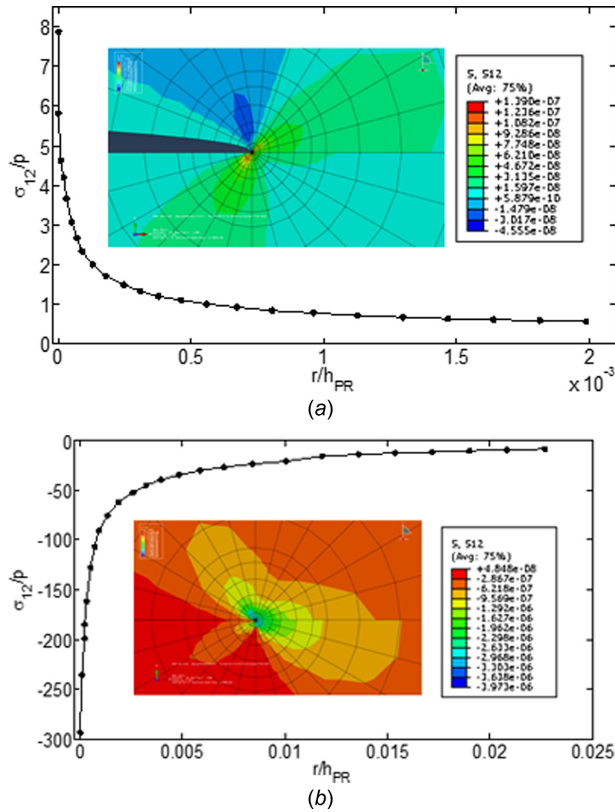

Fig. 7 Distributions of the shear stress straight ahead of the crack front for blister tests with (*a*) a PDMS/photoresist film and (*b*) a bare photoresist film. The insets show the shear stress distribution pattern near the crack front.

controlled by the thickness of the photoresist. The mode-mix increased as the photoresist layer became thicker.

The analysis just conducted (Fig. 5 and Eq. (7)) allowed delamination resistance curves to be obtained from measurements of pressure, crack length, and layer thickness. Figures 8(*a*)–8(*d*) are the resistance curves for graphene/copper, PDMS/copper, graphene/silicon, and PDMS/silicon interfaces, respectively. The mode-mix was 27.0 deg for Figs. 8(*a*) and 8(*b*) and 29.7 deg for Figs. 8(*c*) and 8(*d*). We assume that the presence of graphene had no effect on the mode-mix. Resistance curves for other mode-mixes were also determined by varying the thickness of the photoresist. In all cases, the resistance to delamination grew rapidly from the initiation toughness ($G = \Gamma_0$) to the steady state regime ($G = \Gamma_{ss}$) and then to unsteady growth, represented by the last data point in each resistance curve. Similar resistance curves were also observed in Ref. [4] for bare photoresist and photoresist/graphene films. Here, the initiation toughness of each interface ranged from 0.16 to 0.24 J/m^2 for the graphene/copper interface, from 0.44 to 0.51 J/m^2 for the PDMS/copper interface, from 0.15 to 0.22 J/m^2 for the graphene/silicon interface, and from 0.55 to 0.75 J/m^2 for the PDMS/silicon interface. The corresponding average values of the steady state adhesion energy obtained from all the specimens were 0.346 ± 0.011, 1.094 ± 0.023, 0.402 ± 0.009, and 1.037 ± 0.059 J/m^2, respectively. The extent of delamination growth before achieving steady state was approximately 20 μm for all cases. The total growth was approximately 40 μm for all interfaces except PDMS/copper, which was approximately 70 μm.

The dependence of the steady state adhesion energy on mode-mix was measured for the four interfaces (graphene/copper, graphene/silicon, PDMS/copper, and PDMS/silicon) using five different thicknesses of photoresist; 11, 20, and 41 μm for specimens with PDMS/photoresist laminates, and 15 and 33 μm for bare photoresist. Their mode-mixes were 14 deg, 19 deg, 27 deg, -42 deg, and -30 deg, respectively. Specimens with photoresist thickness less than 10 μm were not considered in order to maintain

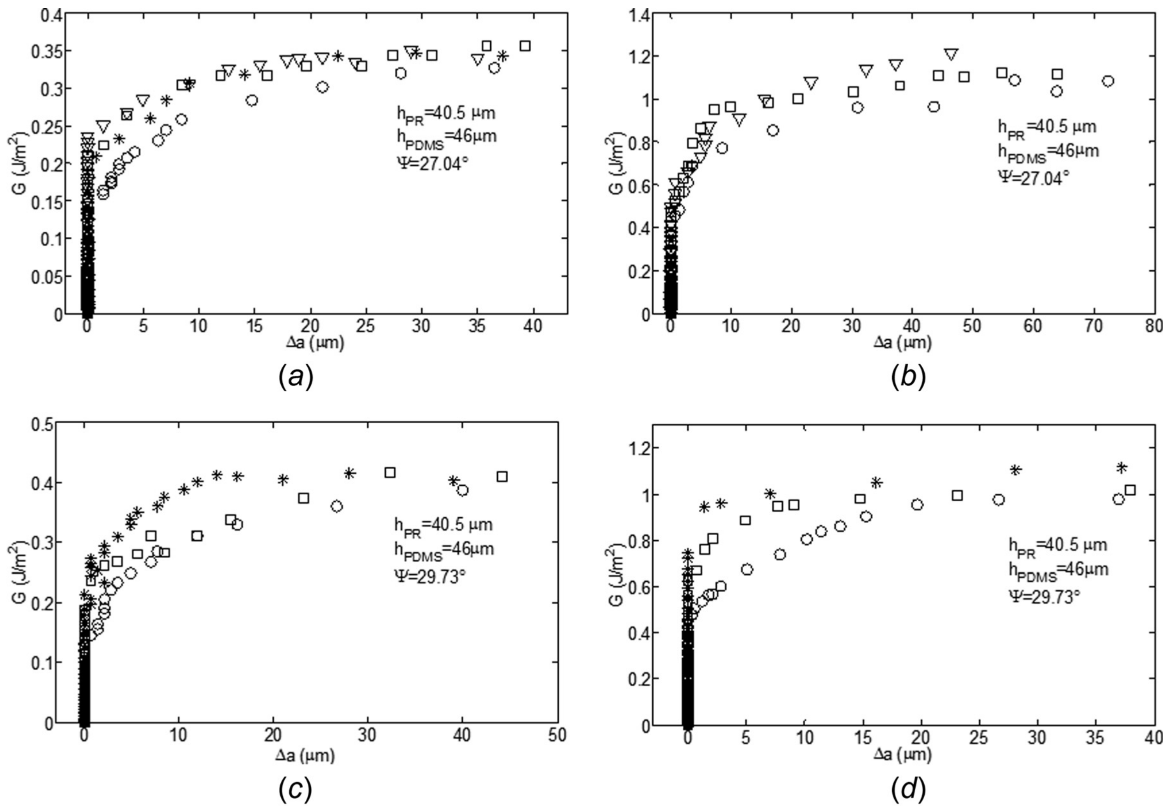

Fig. 8 Resistance curves for (*a*) graphene/copper, (*b*) PDMS/copper, (*c*) graphene/silicon, and (*d*) PDMS/silicon interfaces

Downloaded From: http://appliedmechanics.asmedigitalcollection.asme.org/ on 06/12/2015 Terms of Use: http://asme.org/terms

the central deflection of the blister within the measurement range of the interferometer. The adhesion energy of the graphene/silicon interface was obtained from the current set of experiments as well as the results reported in Ref. [5]. The results (Fig. 9) showed a clear dependence of toughness on mode-mix in all cases. The interfacial toughness increased as the shear stress component became larger. Such increases in interfacial toughness have often been associated with increased plastic dissipation with shear [18,29,30]. However, given the relatively low toughness values encountered in this study, it is unlikely that this was the mechanism here. Asperity locking of rough surfaces in the presence of shear [19] has been proposed as another potential toughening mechanism.

The model developed in Ref. [19] was for a crack in a homogeneous material, but will nonetheless be employed here, given that the moduli of PDMS and photoresist are much lower than those of copper and silicon. The effect of asperity locking on the adhesion energy was given by

$$\frac{\Delta\Gamma_{ss}}{\Gamma_{ss}^0} = \frac{(1-\kappa\alpha_0)\tan^2\psi - \kappa\alpha_0\tan^4\psi}{1+(1+\kappa\alpha_0)\tan^2\psi + \kappa\alpha_0\tan^4\psi} \tag{10}$$

where $\alpha_0 \approx 0.1(EH/\Gamma_{ss}^0)(1-\nu^2)$ and $\kappa = 0.4$ [19]. The parameter α_0 reflects the influence of elastic modulus E and facet height H. Due to asperity locking, the adhesion energy $\Gamma_{ss}(\psi)$ is a function of mode-mix ψ, with $\Delta\Gamma_{ss}(\psi) = \Gamma_{ss}(\psi) - \Gamma_{ss}^0$ and $\Gamma_{ss}^0 = \Gamma_{ss}(0)$.

The approximation that resulted in Eq. (10) is that the facet wavelength and height are the same. The facet height was taken to be the RMS roughness of the copper and silicon surfaces and the values of α_0 for the specimens used in this study are summarized in Table 3. The RMS roughness of the copper and silicon substrates was 4.4 and 0.5 nm, respectively. The mode I toughness Γ_{ss}^0 was obtained for each interface by fitting the measured adhesion energy with Eq. (10), as listed in Table 3. Figure 9 shows the adhesion energy envelopes, comparing the measurements with Eq. (10). It can be seen (Figs. 9(*a*) and 9(*b*)) that the asperity locking model fits the data well for the graphene/copper and graphene/silicon interfaces. The fit for the PDMS/copper interface (Fig. 9(*c*)) and PDMS/silicon interface (Fig. 9(*d*)), which could only be obtained for positive phase angles ($\psi > 0$), was reasonable.

After the graphene/PDMS/photoresist membrane had been blown off from the substrate (copper or silicon), the graphene side of the membrane was inspected by Raman spectroscopy in order to verify that the delamination occurred at the graphene/substrate rather than graphene/PDMS interface. In Ref. [4], the Raman spectra of the graphene side of the photoresist membrane before and after a blister test were reported with the intensity ratio of signatures of graphene G peak (~1583 cm^{-1}) to 2D peak (~2721cm^{-1}), (I_G/I_{2D}) around 1:12. The D peak region

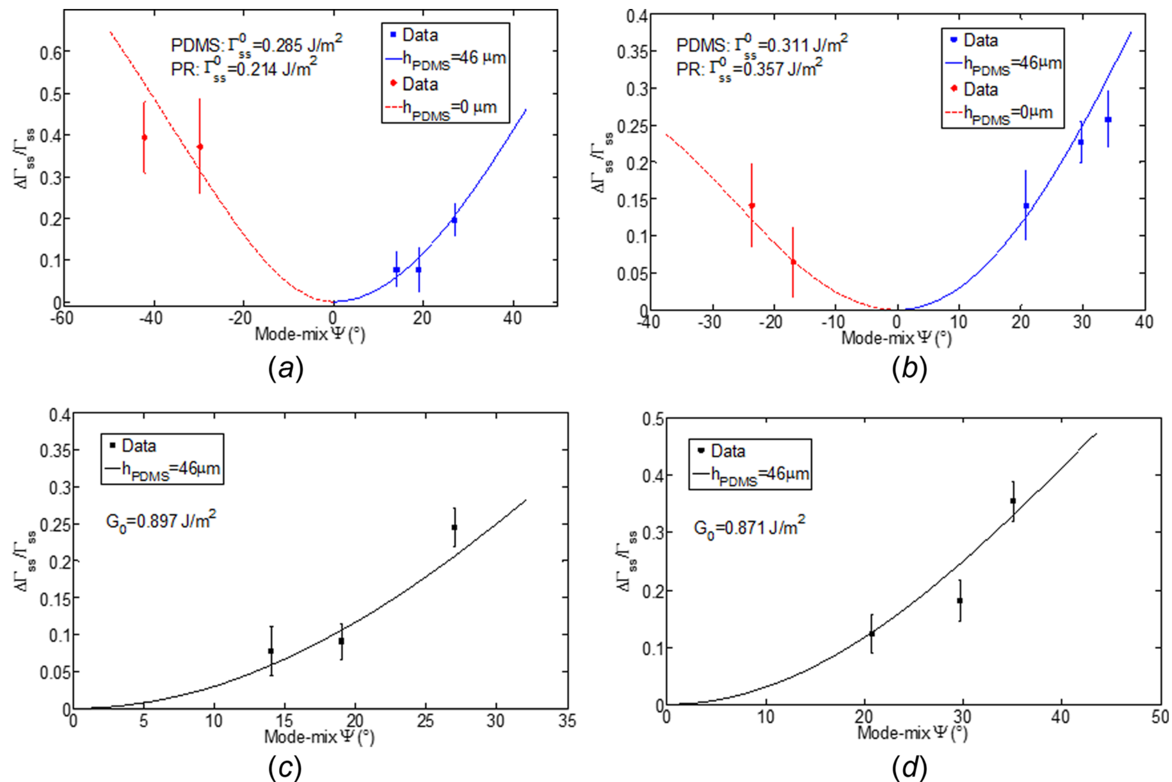

Fig. 9 Toughness envelopes of (*a*) graphene/copper, (*b*) graphene/silicon, (*c*) PDMS/copper, and (*d*) PDMS/silicon interfaces

Table 3 Asperity locking parameters

Interface	Intrinsic toughness G_0 (J/m^2)	RMS roughness H (nm)	Locking parameter α_0
PDMS/graphene/copper	0.285	4.4	9.47×10^{-4}
PR/graphene/copper	0.214	4.4	6.24
PDMS/copper	0.879	4.4	9.47×10^{-4}
PDMS/graphene/silicon	0.311	0.5	9.34×10^{-5}
PR/graphene/silicon	0.357	0.5	0.46
PDMS/silicon	0.871	0.5	9.34×10^{-5}

Downloaded From: http://appliedmechanics.asmedigitalcollection.asme.org/ on 06/12/2015 Terms of Use: http://asme.org/terms

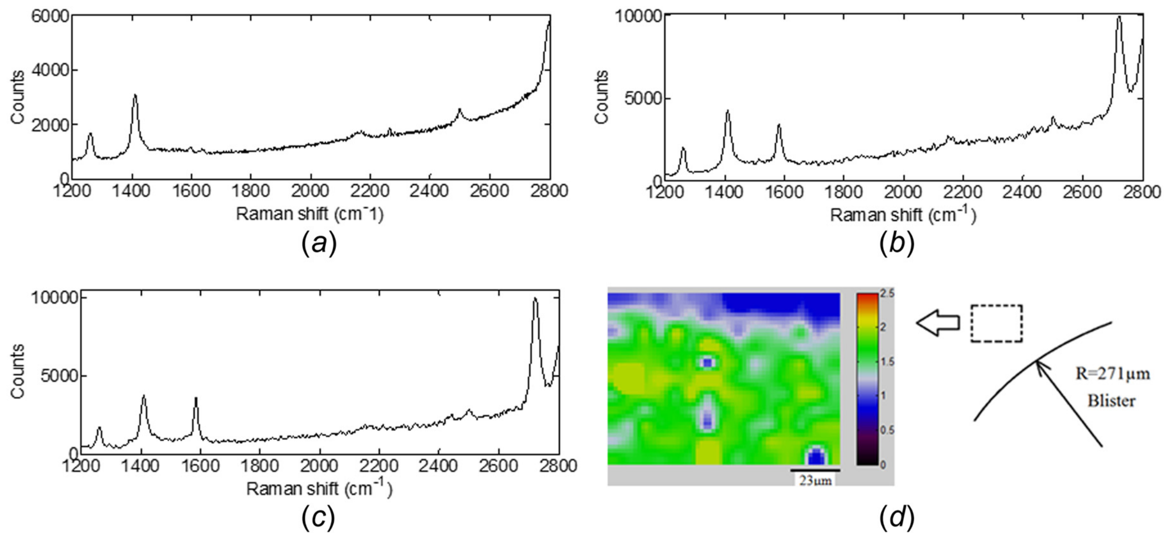

Fig. 10 Raman spectra of (*a*) PDMS and graphene on PDMS/photoresist membranes after blister testing from the (*b*) copper/graphene interface and (*c*) from silicon/graphene interface. (*d*) Raman mapping on a membrane that had delaminated from a copper substrate.

(1350–1380 cm^{-1}), which is used to ascertain the quality of the graphene, was masked by contributions from the photoresist underneath. Thus the results indicated the presence of monolayer graphene on the membrane, but its quality could not be determined.

In order to improve the diagnosis of the delamination path, PDMS was spun between graphene and photoresist. Because PDMS does not contain sp^2 carbon bonding, it does not generate background noise to change the ratio of the G to 2D peak intensities. Figure 10 shows the Raman spectra of (*a*) PDMS and the graphene surfaces of PDMS/photoresist membrane after delamination from (*b*) a copper substrate and (*c*) a silicon substrate. Each spectrum was itself an average of three runs. The spectrum of a bare PDMS surface (Fig. 10(*a*)) confirmed that it did not have any peaks near the G and 2D peaks of graphene. There were some peaks near the graphene D peak, thereby leaving open the possibility of D peak masking. Peaks from PDMS on graphene delaminated from copper (Fig. 10(*b*)) and silicon (Fig. 10(*c*)) indicated that the graphene had been successfully transferred to PDMS. The G and 2D peaks occurred at 1586 and 2724 cm^{-1} for delamination from copper and 1592 and 2727 cm^{-1} for silicon, respectively. Such a minor difference might be due to residual stresses in graphene [31]. The ratio of the peak intensities (I_{2D}/I_G) is 3:1 for high quality graphene on silicon, and the value obtained here was 2.3:1, which indicates that the graphene under the beam spot was a monolayer and free of defects as indicated by absence of the D peak. Figure 10(*d*) is a Raman map of the ratio in a region near the hole with an average value of 1.8. In most areas, the ratio was approximately 2, which is indicative of monolayer graphene. In a very few spots, the ratio was less than 1; these could correspond to small flakes of multilayer graphene formed during the CVD process. Thus the characterization of the fracture surfaces by Raman spectroscopy confirmed that graphene had indeed been successfully transferred from the copper and silicon substrates to PDMS.

5 Conclusions

The dependence of the adhesion energy between CVD grown graphene and copper and silicon substrates to which it had been transferred was determined by blister tests that made use of composite backing layers made up of PDMS and photoresist in order to vary the ratio of shear-to-tensile stresses or the fracture mode-mix at the interface. The use of PDMS next to the graphene was particularly useful in extending the range of the mode-mix that is typically accessible to blister tests as well as removing ambiguities in Raman spectra that arise when using epoxies. For both copper and silicon substrates, it was found that the adhesion energy between them and graphene was strongly dependent on the fracture mode-mix in spite of the fact that all materials were behaving elastically during delamination. This led to the conclusion that asperity locking due to the surface roughness of the substrates is responsible for the noted mode-mix dependence of the adhesion energy.

Acknowledgment

One of the authors (Z.C.) acknowledges many fruitful discussions with Dr. Wei Gao regarding modeling issues. The authors gratefully acknowledge partial financial support of this work by the National Science Foundation through Grant No. CMMI-1130261. This work was also based upon work supported in part by the National Science Foundation under Cooperative Agreement No. EEC-1160494. Any opinions, findings and conclusions or recommendations expressed in this material are those of the author(s) and do not necessarily reflect the views of the National Science Foundation.

References

[1] Zong, Z., Chen, C. L., Dokmeci, M. R., and Wan, K. T., 2010, "Direct Measurement of Graphene Adhesion on Silicon Surface by Intercalation of Nanoparticles," J. Appl. Phys., **107**(2), p. 026104.

[2] Koenig, S. P., Boddeti, N. G., Dunn, M. L., and Bunch, J. S., 2011, "Ultrastrong Adhesion of Graphene Membranes," Nat. Nanotechnol., **6**(9), pp. 543–546.

[3] Boddeti, N. G., Koenig, S. P., Long, R., Xiao, J., Bunch, J. S., and Dunn, M. L., 2013, "Mechanics of Adhered, Pressurized Graphene Blisters," ASME J. Appl. Mech., **80**(4), p. 040909.

[4] Cao, Z., Wang, P., Gao, W., Tao, L., Suk, J. W., Ruoff, R. S., Akinwande, D., Huang, R., and Liechti, K. M., 2014, "A Blister Test for Interfacial Adhesion of Large-Scale Transferred Graphene," Carbon, **69**, pp. 390–400.

[5] Na, S. R., Suk, J. W., Ruoff, R. S., Huang, R., and Liechti, K. M., 2014, "Ultra Long-Range Interactions Between Large Area Graphene and Silicon," ACS Nano, **8**(11), pp. 11234–11242.

[6] Yoon, T., Shin, W. C., Kim, T. Y., Mun, J. H., Kim, T. S., and Cho, B. J., 2012, "Direct Measurement of Adhesion Energy of Monolayer Graphene As-Grown on Copper and Its Application to Renewable Transfer Process," Nano Lett., **12**(3), pp. 1448–1452.

[7] Na, S. R., Suk, J. W., Tao, L., Akinwande, D., Ruoff, R. S., Huang, R., and Liechti, K. M., 2015, "Selective Mechanical Transfer of Graphene From Seed Copper Foil Using Rate Effects," ACS Nano, **9**(2), pp. 1325–1335.

[8] He, Y., Chen, W. F., Yu, W. B., Ouyang, G., and Yang, G. W., 2013, "Anomalous Interface Adhesion of Graphene Membranes," Sci. Rep., **3**, p. 2660.

[9] Bunch, J. S., and Dunn, M. L., 2012, "Adhesion Mechanics of Graphene Membranes," Solid State Commun., **152**(15), pp. 1359–1364.

[10] Chadegani, A., and Batra, R. C., 2011, "Analysis of Adhesive-Bonded Single-Lap Joint With an Interfacial Crack and a Void," Int. J. Adhes. Adhes., **31**(6), pp. 455–465.

[11] Liu, Y. J. J., and Xu, N., 2000, "Modeling of Interface Cracks in Fiber-Reinforced Composites With the Presence of Interphases Using the Boundary Element Method," Mech. Mater., **32**(12), pp. 769–783.

Downloaded From: http://appliedmechanics.asmedigitalcollection.asme.org/ on 06/12/2015 Terms of Use: http://asme.org/terms

[12] Ye, T., Suo, Z., and Evans, A. G., 1992, "Thin-Film Cracking and the Roles of Substrate and Interface," Int. J. Solids Struct., **29**(21), pp. 2639–2648.
[13] Hutchinson, J. W., and Suo, Z., 1991, "Mixed Mode Cracking in Layered Materials," Adv. Appl. Mech., **29**, pp. 63–191.
[14] Gerstner, R. W., and Dundurs, J., 1969, "Representation of Stress Concentration Factors for a Composite in Plane Strain," J. Compos. Mater., **3**(1), pp. 108–115.
[15] Rice, J. R., 1988, "Elastic Fracture Mechanics Concepts for Interfacial Cracks," ASME J. Appl. Mech., **55**(1), pp. 98–103.
[16] Suo, Z., and Hutchinson, J., 1990, "Interface Crack Between Two Elastic Layers," Int. J. Fract., **43**(1), pp. 1–18.
[17] Wang, J. S., and Suo, Z., 1990, "Experimental-Determination of Interfacial Toughness Curves Using Brazil-Nut-Sandwiches," Acta Metall. Mater., **38**(7), pp. 1279–1290.
[18] Chai, Y. S., and Liechti, K. M., 1992, "Asymmetric Shielding in Interfacial Fracture Under In-Plane Shear," ASME J. Appl. Mech., **59**(2), pp. 295–304.
[19] Evans, A. G., and Hutchinson, J. W., 1989, "Effects of Non-Planarity on the Mixed Mode Fracture Resistance of Bimaterial Interfaces," Acta Metall., **37**(3), pp. 909–916.
[20] Swadener, J. G., and Liechti, K. M., 1998, "Asymmetric Shielding Mechanisms in the Mixed-Mode Fracture of a Glass/Epoxy Interface," ASME J. Appl. Mech., **65**(1), pp. 25–29.
[21] Han, X. L., Ellyin, F., and Xia, Z. H., 2001, "Interface Crack Between Two Different Viscoelastic Media," Int. J. Solids Struct., **38**(44–45), pp. 7981–7997.
[22] Jensen, H. M., and Thouless, M. D., 1993, "Effects of Residual Stresses in the Blister Test," Int. J. Solids Struct., **30**(6), pp. 779–795.
[23] Jensen, H. M., 1998, "Analysis of Mode Mixity in Blister Tests," Int. J. Fract., **94**(1), pp. 79–88.
[24] Li, X., Cai, W., An, J., Kim, S., Nah, J., Yang, D., Piner, R., Velamakanni, A., Jung, I., Tutuc, E., Banerjee, S. K., Colombo, L., and Ruoff, S., 2009, "Large-Area Synthesis of High-Quality and Uniform Graphene Films on Copper Foils," Science, **324**(5932), pp. 1312–1314.
[25] Suk, J. W., Kitt, A., Magnuson, C. W., Hao, Y., Ahmed, S., An, J., Swan, A. K., Goldberg, B. B., and Ruoff, R. S., 2011, "Transfer of CVD-Grown Monolayer Graphene Onto Arbitrary Substrates," ACS Nano, **5**(9), pp. 6916–6924.
[26] Wang, P., Gao, W., Cao, Z., Liechti, K. M., and Huang, R., 2013, "Numerical Analysis of Circular Graphene Bubbles," ASME J. Appl. Mech., **80**(4), p. 040905.
[27] Shih, C. F., and Asaro, R. J., 1988, "Elastic–Plastic Analysis of Cracks on Bimaterial Interfaces: Part I—Small Scale Yielding," ASME J. Appl. Mech., **55**(2), pp. 299–316.
[28] Hopcroft, M., Kramer, T., Kim, G., Takashima, K., Higo, Y., Moore, D., and Brugger, J., 2005, "Micromechanical Testing of SU-8 Cantilevers," Fatigue Fract. Eng. Mater. Struct., **28**(8), pp. 735–742.
[29] Swadener, J. G., and Liechti, K. M., 1998, "Asymmetric Shielding Mechanisms in the Mixed-Mode Fracture of a Glass/Epoxy Interface," ASME J. Appl. Mech., **65**(1), pp. 25–29.
[30] Swadener, J. G., Liechti, K. M., and de Lozanne, A. L., 1999, "The Intrinsic Toughness and Adhesion Mechanisms of a Glass/Epoxy Interface," J. Mech. Phys. Solids, **47**(2), pp. 223–258.
[31] Ni, Z. H., Yu, T., Lu, Y. H., Wang, Y. Y., Feng, Y. P., and Shen, Z. X., 2008, "Uniaxial Strain on Graphene: Raman Spectroscopy Study and Band-Gap Opening," Acs Nano, **2**(11), pp. 2301–2305.

Downloaded From: http://appliedmechanics.asmedigitalcollection.asme.org/ on 06/12/2015 Terms of Use: http://asme.org/terms